atmosphere

MDPI

Article

Physicochemical Assessment of the Road Vehicle Traffic Pollution Impact on the Urban Environment

Marcel Rusca [1], Tiberiu Rusu [1], Simona Elena Avram [1], Doina Prodan [2], Gertrud Alexandra Paltinean [2,*], Miuta Rafila Filip [2], Irina Ciotlaus [2], Petru Pascuta [1], Tudor Andrei Rusu [1] and Ioan Petean [3,*]

[1] Faculty of Materials and Environmental Engineering, Technical University of Cluj-Napoca, 400641 Cluj-Napoca, Romania
[2] Raluca Ripan Institute for Research in Chemistry, Babeș-Bolyai University, 400294 Cluj-Napoca, Romania
[3] Faculty of Chemistry and Chemical Engineering, Babes-Bolyai University, 400028 Cluj-Napoca, Romania
* Correspondence: gertrud.paltinean@ubbcluj.ro (G.A.P.); ioan.petean@ubbcluj.ro (I.P.)

Abstract: Vehicle traffic pollution requires complex physicochemical analysis besides emission level measuring. The current study is focused on two campaigns of emissions measurements held in May and September 2019 in Alba Iulia City, Romania. There was found a significant excess of $PM_{2.5}$ for all measuring points and PM_{10} for the most circulated points during May, along with significant VOC and CO_2 emissions. September measurements reveal threshold excess for all PM along with increased values for VOC and CO_2 emissions. These are the consequences of the complex environmental interaction of the traffic. Street dust and air-suspended particle samples were collected and analyzed to evidence the $PM_{2.5}$ and PM_{10} sources. Physicochemical investigation reveals highly mineralized particulate matter: $PM_{2.5}$ fractions within air-suspended particle samples predominantly contain Muscovite, Kaolinite, and traces of Quartz and Calcite, while PM_{10} fractions within air-suspended particle samples predominantly contain Quartz and Calcite. These mineral fractions originate in street dust and are suspended in the atmosphere due to the vehicles' circulation. A significant amount of soot was found as small micro-sized clusters in $PM_{2.5}$ and fine micro-spots attached over PM_{10} particles, as observed by Mineralogical Optical Microscopy (MOM) and Fourier Transformed Infrared Spectroscopy (FTIR). GC-MS analysis found over 53 volatile compounds on the investigated floating particles that are related to the combustion gases, such as saturated alkanes, cycloalkanes, esters, and aromatic hydrocarbons. It proves a VOC contamination of the measured particulate matters that make them more hazardous for the health. Viable strategies for vehicle traffic-related pollutants mitigation would be reducing the street dust occurrence and usage of modern catalyst filters of the combustion gas exhausting system.

Keywords: $PM_{2.5}$; PM_{10}; volatile organic compounds; physicochemical analysis

Citation: Rusca, M.; Rusu, T.; Avram, S.E.; Prodan, D.; Paltinean, G.A.; Filip, M.R.; Ciotlaus, I.; Pascuta, P.; Rusu, T.A.; Petean, I. Physicochemical Assessment of the Road Vehicle Traffic Pollution Impact on the Urban Environment. *Atmosphere* **2023**, *14*, 862. https://doi.org/10.3390/atmos14050862

Academic Editors: Dušan Jandačka and Daniela Ďurčanská

Received: 12 April 2023
Revised: 9 May 2023
Accepted: 10 May 2023
Published: 11 May 2023

1. Introduction

Nowadays, air quality is one of the most discussed research topics worldwide. Particulate matter (PM) and volatile organic compounds (VOCs) generated in the atmosphere by road traffic and socio-industrial activities are situated among the main pollutants [1,2]. PM_{10} and $PM_{2.5}$ are particles with aerodynamic diameters equal to or less than 10 µm and, respectively, 2.5 µm, retaining on their surface other toxic substances such as heavy metals (Pb, Cd, Ni, As), cigarette ash, exhaust gases, polycyclic aromatic hydrocarbons (PAH), viruses, pollen, bacteria, and other organic components [3–6].

Most of the PMs related to road vehicle traffic have two sources: the natural one, such as street dust, which is highly mineralized due to the soil particles [7,8], and the particles directly generated by car exhausts, such as soot and other combustion residues [9,10]. Another PM component related to vehicle circulation is the oxide material coming in from the cars' chassis rust [11].

These PMs combined with dangerous organic compounds may affect environmental aspects, such as climate change, the greenhouse effect, thinning of the ozone layer due to their toxic effect on the plants and tree leaves, which further affects the oxygen balance in the local atmosphere [12,13]. Mammals are also very exposed to the risk due to contaminated PM penetration into the respiratory system causing respiratory diseases, such as asthma and silicosis [14,15], pulmonary cancer [16,17], and cardiovascular diseases [18,19], which induce long-time illness until death. Nitrogen and sulfur oxide emissions into the atmosphere facilitate acid rain formations that might affect PM sources (e.g., street dust) composition increasing their hazardous potential [20].

The finest PMs are more hazardous due to their ability to be suspended in the atmosphere for a long time and to travel at long distances along with air currents [21]. Rapid urbanization, which implies an increase in combustion vehicle number (sometimes more than one car/family), also generates particulate matter via tire wear and interaction with street dust that induces fine mineral fraction suspension into the atmosphere [22] along with large amounts of exhausting gases and soot emission into the air [23].

VOCs are chemical compounds originating from fuel combustion and industry, such as benzene, ethylbenzene, toluene, hexanal, acetone, iso-pentane, formaldehyde, acetaldehyde, and xylenes, which, through a chemical reaction with other compounds in the atmosphere, contributed to ozone formation into the troposphere (which is very dangerous for living beings), photochemical smog, and secondary organic aerosols. VOCs are debated in the specialized literature because they distort the quality of the air and produce increased risks for human health leading to pathologies, such as asthma, atopic dermatitis, neurological, respiratory, cardiovascular, disorders irritations, allergies, and cancer [24,25].

The literature data show that atmospheric PM pollution remains responsible for the unfavorable development of all ecosystems, causing a very large number of deaths; 6.7 million casualties were reported only in 2019 [26]. This fact is also facilitated by population comorbidities (e.g., diabetes, arterial hypertension, asthma, and silicosis), which are sensitive to short-term and long-term exposure to the finest PM fractions.

Due to these consequences, laws, and directives were implemented, imposing mandatory limit thresholds and measurement protocols in order to maintain an environment as clean as possible: Directive 2008/50/EC; Council Directive 1999/30/EC; and Romanian Law No. 104 of 15 June 2011 regarding Ambient Air Quality, updated on 22 May 2015 [27–29]. Thus, Table 1 shows the limit threshold values for PM_{10}, $PM_{2.5}$, NO_2, SO_2, CO, Benzene, and Pb.

Table 1. Atmospheric pollutants limits according to actual legislation.

Pollutants	Period	Concentration	Refs.
PM_{10}	24 h	50 $\mu g/m^3$	[27–29]
	Annual	40 $\mu g/m^3$	
$PM_{2.5}$	24 h	25 $\mu g/m^3$	[27–29]
	Annual	20 $\mu g/m^3$	
NO_2	Annual	40 $\mu g/m^3$	[27–29]
SO_2	24 h	125 $\mu g/m^3$	[27–29]
CO	8 h	10 mg/m^3	[27–29]
C_6H_6	Annual	5 $\mu g/m^3$	[27–29]
Pb	Annual	0.5 $\mu g/m^3$	[27–29]

These measures educate and stimulate the authorities and civil society: to be aware of the danger degree, how to protect the ecosystems from harmful anthropogenic actions, and to intensify research regarding the harmful potential of atmospheric pollution [30].

According to Directive 2008/50/EC, the European Commission proposed two stages of changing the limit thresholds for $PM_{2.5}$, meaning that from 1 January 2015, the maximum limit is 25 $\mu g/m^3$, and, from 1 January 2020, the threshold limit for fine fractions should be 20 $\mu g/m^3$ (value not yet implemented in all regional actual laws). The air quality index

(AQI) was introduced for a facile population to be informed about the quality of the air they breathe and to warn about any hazard risks. In Romania, this codification system of the National Air Quality Monitoring Network establishes the danger degree of suspended particles. Air quality is deteriorating over the limit of 50 $\mu g/m^3$ for PM_{10}, respectively 25 $\mu g/m^3$ for $PM_{2.5}$ when the AQI becomes bad. It becomes very bad when a threshold is significantly exceeded. People with co-morbidities, as well as children, should avoid long-term exposure to such an atmosphere [31].

This research is based on the correlation between the pollutant emissions values measured in the field in Alba Iulia City with the physicochemical investigations carried out on collected samples: street dust and air-suspended particles collected from the atmosphere in the adjacent area of the emission measurement points. The aim is to highlight the microstructural and morphological aspects, chemical bonds, and potentially harmful compounds which might influence the environmental parameters measured on the sites of interest.

2. Materials and Methods

2.1. Environmental Parameter Measuring and Sampling

The current article represents a part of a wide environmental research regarding atmospheric pollution in Alba Iulia City, Romania, developed over several months in 2019. The most important zones for environmental parameters measuring were identified and marked on the map in Figure 1.

Figure 1. Geographical placement of the zones targeted for the environmental parameters measuring [Google Maps display, GPS coordinates 46.07328° N; 23.58029° E].

There are some zones with several measuring points, and other zones have a single measuring point:

Zone 1: Point P1—Tudor Vladimirescu Street;

Point P2—Calea Moţilor Street;
Point P3—Tudor Vladimirescu Street;

Zone 2: Point P4—Ferdinand Boulevard (Exit to Sebeș);
Zone 3: Point P5—Railway Station Square and Bus Station;

Zone 4: Point P6—Hotel Cetate;
Point P7—Central Park;
Zone 5: Point P8—Horea Boulevard;
Point P9—Unirii Street;
Point P10—Closca Street (Exit to Cluj);
Point P11—Dedeman Market;
Point P12—OMV Gas station.

VOC and CO_2 emissions into the atmosphere were measured using a portable device UNI-T UT 338C Air Quality Meter produced by UNI-T Company, Augsburg, Germany. PM_{10} and $PM_{2.5}$ levels in the atmosphere were measured with a portable aerosol monitor DUST TRAK DRX produced by TSI Company, Aachen, Germany. The total measuring time for each point was 10 min, three different readings were effectuated, and the mean value was considered representative of the evaluation of vehicle traffic-related emissions. All measured values were statistically processed, and mean values and their standard deviation were determined. Statistical relevance between collecting points and legal thresholds was investigated using the Anova One-Way test, and the differences among mean values of each collecting point were evidenced by the Tukey post hoc test. Statistical procedures were effectuated using Origin 2019b Graphic and Analysis Software, Microcal Software Inc., Northampton, MA, USA.

The number of passing vehicles during measurement time was counted. The temperature at the soil level and the wind speed were also measured as weather indicators. These measurements were effectuated in two distinct campaigns: the first was effectuated on 31 May 2019, and the second was performed on 30 September 2019.

Statistical analysis of the measured values indicates that the most polluted points with particulate matter are P3—Tudor Vladimirescu Street and P10—Closca Street (Exit to Cluj). These points were considered for material sampling. An average representative sample of street dust was collected from these sites. SD1 was collected from the P3 point, and SD2 was collected from P10. Air-suspended particle (ASP)-collecting boxes were placed on these two sites from May to the end of September, and the collected powders were considered for analysis. Therefore, air-suspended particles collected from the P3 point became representative sample ASP1, and those collected from the P10 point became representative sample ASP2.

2.2. Physicochemical Investigation Methods

X-ray diffraction (XRD) was effectuated with an XRD-6000 Shimadzu Diffractometer produced by Shimadzu Company, Tokyo, Japan, using monochromatic Cuk_{α} radiation with wavelength λ = 1.540560 Å. The patterns were registered at room temperature in the range of 20–70 degrees 2 theta. Crystalline phases and compounds were identified using Match 1.0 soft equipped with PDF2 database package, Crystal Impact Company, Bonn, Germany.

Mineralogical optical microscopy (MOM) was effectuated using a Laboval 2 Microscope produced by Carl Zeiss, Oberkochen, Germany, under the cross-polarized light inspection of the samples. The images were acquired with a digital camera of 10 megapixels produced by Samsung, Seoul, Korea.

Scanning electron microscopy (SEM) was effectuated with Inspect™ SEM microscope produced by FEI Company, Hillsboro, OR, USA. Particulate matter samples SD and FP were deposited onto a double adhesive carbon disk for proper particle immobilization and investigated in low-vacuum mode at an acceleration voltage of 20 kV.

Fourier Transformed Infrared Spectroscopy (FTIR) was effectuated with a JASCO—610 spectrophotometer produced by JASCO International Co., Ltd., Tokyo, Japan. Each spectrum was registered in the range of 400–4000 cm^{-1} in order to evidence the specific absorption bands related to the chemical compounds within SD and ASP samples.

Each of the particulate matter powders was embedded into a potassium bromide pellet for an optimal infrared investigation.

Gas Chromatography–Mass Spectrometry (GC-MS) was effectuated on an Agilent GC-MS Gas Chromatograph-7890A/5975/2008 (Agilent Technologies, Inc. Europe, Waldbronn, Germany) was used for analysis. The ASP samples (0.5 g) were diluted in 2 mL solvents (dichloromethane: hexane = 1:3) mixture for 30 min, then they were ultrasound-treated for 6 min and then centrifuged at 4400 rpm for 15 min. The volatile fraction was filtered and concentrated, and 1 µL was injected in GC-MS. The analyses were performed in scan mode on a DB-5MS (30 m × 0.25 mm × 0.25 µm) capillary column (Agilent 19091S-433M), high purity He carrier gas at a flow rate of 1 mL/min. Temperature program: initial temperature 40 °C with a ramp rate of 5 °C/min up to 300 °C, injection volume of 1 µL, 100:1 split ratio, MS 70 eV, mass range u.a.m. 40–500. Data acquisition and processing were performed using MSD Chem Station software. The NIST L14 library was used for the identification/confirmation of the structure components. In addition, a C8–C20 standards alkanes (Alkane Standard Solution C8–C20, Sigma-Aldrich, Darmstadt, Germany) were used for the calculation of the linear retention index (LRI) and matching the experimental values with those reported in the literature for similar chromatographic columns in the same condition. The qualitative analysis was based on the integrated area of compound peaks.

3. Results and Discussion

3.1. Environmental Parameter Measurements

Auto vehicle traffic pollution strongly depends on the local circulation characteristic, such as the number of cars per time unit, their relative speed, and the weather parameters, such as air temperature and wind speed. Vehicle circulation speed directly influences the particulate matter sources by street dust engaging into the atmosphere as floating particles [7,8] the PM emission is directly proportional to the car speed. Tires also act as milling bodies that cause intensive fragmentation of silicate particles, such as Quartz, and clays, such as Muscovite and Kaolinite. The literature data proves that the clay particles fragmentation under road traffic conditions generates a lot of submicron particles that are related to the PM_1 category (e.g., particulate matter with an aerodynamic diameter of 1 µm and below) [32]; the advanced particle clay refinement under mechanical solicitation is also described by Zhang et al. [33].

The other aspect related to the car's high speed is a relatively lower amount of combustion gas emission per atmospheric volume unit due to their intensive dissipation. Street dust engaging into the atmosphere is significantly reduced at low car speeds, but the combustion gas emissions tend to increase due to slow vehicle movement [34]. A natural source of atmospheric particulate matter related to street dust is wind speed. In certain conditions, the air currents might engage into the atmosphere the street dust, generating local pollution in the absence of vehicle traffic [35,36].

The environmental parameters measured in May 2019 campaign are centralized in Table 2. The weather conditions during measurements day (31 May 2019) were moderate: cloudy sky and very low wind speed in the morning and partly sunny sky and low wind speed. Temperature ranges from 23.2 to 24.7 °C. Similar weather conditions were observed three consecutive days before starting measurements. Therefore, the weather conditions are good and prevent particulate matter emissions due to the natural sources.

The measured values, Table 2, show that the most polluted measuring point is P3 which reveals a strong exceeding of the limits for $PM_{2.5}$; PM_{10} and VOC for the Tudor Valdimirescu Street in the close proximity of the intersection with Calea Motilor Street. A number of 65 vehicles pass through the measuring point in 10 min, which confirms that it is an agglomerated intersection which implies average car speed. The second most polluted measuring point is P10, also having gross exceeding of the limit values. This zone is situated around the exit to Cluj, a place associated with intensive car traffic. This fact has been proved by those 50 vehicles counted in 10 min. The speed is relatively intense there because of the proximity of the point, which allows increasing the speed limit from 40 km/h to

70 km/h. This agglomerated urban traffic condition requires more detailed investigations to trace physical and chemical evidence between mineral and organic particles involved in the measured pollutants.

Table 2. Atmospheric pollutants measured in May 2019 campaign.

M.P.	$PM_{2.5}$, $\mu g/m^3$	PM_{10}, $\mu g/m^3$	VOC, $\mu g/m^3$	CO_2, ppm	Vehicles/10 min., Counts	Air Temp., °C	Wind Speed, m/s
1	38 ± 1.2	36 ± 0.5	6.8 ± 1.6	608 ± 13.22	59	23.2	0.18–0.85
2	28 ± 1.1	38 ± 1.1	0.5 ± 0.0	556 ± 5.03	48	23.2	0.18–0.85
3 *	49 ± 0.5	55 ± 1.2	1.2 ± 0.5	558 ± 25.05	65	21.2	1.4
4	36 ± 1.8	48 ± 1.7	1.6 ± 0.0	556 ± 10.26	46	23.6	0.85–1.45
5	32 ± 0.6	33 ± 0.3	0.2 ± 0.1	550 ± 0.09	57	23.6	0.85–1.45
6	36 ± 1.4	31 ± 0.8	0.4 ± 25	580 ± 22.81	55	23.6	0.85–1.45
7	38 ± 0.3	41 ± 1.8	0.2 ± 0.0	539 ± 15.69	44	24.1	0.85–1.45
8	36 ± 1.7	40 ± 0.5	0.4 ± 0.0	560 ± 3.05	57	24.7	0.85–1.45
9	42 ± 1.9	45 ± 1.7	0.2 ± 0.0	552 ± 25.32	48	24.7	0.85–1.45
10 *	46 ± 1.4	30 ± 1.4	0.4 ± 0.0	638 ± 15.09	50	24.7	0.85–1.45
11	34 ± 2	32 ± 1.4	0.2 ± 0.0	525 ± 20.20	44	24.7	0.85–1.45
12	38 ± 0.6	36 ± 1.3	0.2 ± 0.1	506 ± 5.04	44	24.7	0.85–1.45
Mean	37.75	38.75	1.025	560.64	51.41	-	-
p	9.89×10^{-16}	1.77×10^{-12}	4.81×10^{-13}	4.30×10^{-8}	-	-	-

* significant statistical difference.

The opposite situations with relatively low amounts of particulate matter and VOC emissions are observed for measuring points P2; P11; P5; P4; P6. These points belong both to the residential areas, such as Hotel Cetate and Central Park, and economic activities areas, such as Railway Station Square and Bus Station or Dedeman Market. Some of the literature data mention lower levels of particulate matter pollution in residential areas [37,38], but, in fact, the values are related to the low traffic. Measurements effectuated in the May campaign show that the pollutant emission level is strongly dependent on the number of cars per 10 min. Unfortunately, all measured values exceed the legal limits, and the discussion is limited to where is placed higher and lower exceeding.

Anova statistical analysis for $PM_{2.5}$ sustains the significant differences for all 12 measuring points reported to the legal threshold by a *p*-value of <0.05. Tukey's post hoc test reveals less statistical difference for points P2 and P5, and the most significant difference regarding the legal threshold is observed for points P3 and P10. Anova and Tukey's post hoc test results regarding PM_{10} reported to the legal threshold show that there are significant statistical differences for all measuring points except P2, P4, and P9. Both $PM_{2.5}$ and PM_{10} statistical variances strongly depend on the traffic conditions, which is in agreement with the literature [39,40].

Statistical results regarding VOC measured values indicate that all measuring points except P1 and P4 present significant differences ($p < 0.05$) corresponding to the exceeding of the legal threshold. Anova test regarding CO_2 values reveals strong differences among all 12 measuring points and the legal threshold, the most relevant as pollution level being P1 and P10.

The measured values evidence a strong connection between vehicle traffic and PM emissions into the atmosphere. However, the data set is valid only for the measuring day unless it represents a component of a repetitive pattern. Both points P3 and P10 are situated in the action range of the governmental automated Air Quality Monitoring Station (AQMS) operated by Alba County Environmental Agency but at a certain distance. PM_{10} monthly values measured with the automated station are available in Figure 2.

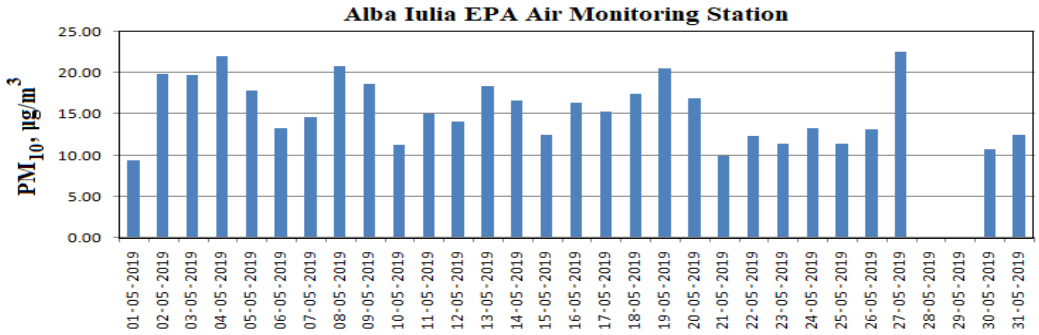

Figure 2. PM_{10} level variation during May 2019, according to Alba Iulia Environmental Protection Agency, measured with the automated Air Quality Monitoring Station.

Therefore, values measured in May are as follows: mean value 15.46 µg/m^3; minimum 9.36 µg/m^3; maximum 22.53 µg/m; and daily value for 31 May 2019 is 12.45 µg/m^3. A certain pattern is observed: high values on Monday and Friday due to the intensive traffic and lower values during the weekend. The 31 May 2019 was a Friday, explaining the vehicle pass rate of 6.5/minute at the measuring point P3. However, the values measured by the AQMS are significantly lower than our measured values. This is explained by the average distance between our measuring point and the AQMS, the pollutant concentration decreases from the emission point (where we effectuate measurements) to the AQMS position.

The environmental parameters measured in September 2019 campaign are centralized in Table 3.

Table 3. Atmospheric pollutants measured in September 2019 campaign.

M.P.	$PM_{2.5}$, µg/m^3	PM_{10}, µg/m^3	VOC, µg/m^3	CO_2, ppm	Vehicles/10 min., Counts	Temperature, °C	Wind Speed, m/s
1 *	70 ± 3.7	95 ± 5.3	6.4 ± 1.5	608 ± 10.4	74	15.1	0.1–0.45
2 *	70 ± 1	93 ± 3	9.0 ± 3.0	686 ± 11	73	12	0.2–0.4
3 *	68 ± 2.6	90 ± 5.5	4.1 ± 0.3	448 ± 5.3	68	14.7	0.15–0.35
4 *	63 ± 3.2	72 ± 3.2	3.1 ± 0.3	448 ± 0.6	64	17.1	0.15–0.3
5	35 ± 3.7	42 ± 0.5	0.2 ± 0.1	445 ± 10.4	48	15.2	0.18–0.35
6	30 ± 2	36 ± 2.5	0.2 ± 0.2	597 ± 18.6	-	20.1	0.2
7	35 ± 0.6	41 ± 3	0.2 ± 0	399 ± 21.5	-	23	0.15
8	40 ± 4	44 ± 1	1.6 ± 0.3	415 ± 10.4	48	23	0.2–0.3
9	35 ± 1.7	40 ± 3.2	0.2 ± 0.1	405 ± 25.8	-	23	0.2–0.3
10 *	68 ± 3.2	87 ± 1.1	1.4 ± 0.5	562 ± 22.1	74	23	0.2–0.5
11	49 ± 1.1	64 ± 1.5	1.1 ± 0.1	439 ± 18.9	-	23	0.25
12	46 ± 5	56 ± 5.6	2.5 ± 0.4	429 ± 21.1	63	23	0.25
Mean	50.75	63.33	2.500	490.08	42.66	-	-
p	1.71×10^{-16}	8.08×10^{-19}	3.09×10^{-10}	3.24×10^{-16}	-	-	-

* significant statistical difference.

The weather is characteristic of the end of the summer and the beginning of the autumn. The sky was partly cloudy all day without precipitations, and temperature ranged from 12 to 23 °C, and wind speed was moderate in the morning and 0.1–0.5 m/s during the rest of the day. Similar weather conditions were observed for three days before measurements.

Values measured in the September campaign, Table 3, evidence a considerable increase in the particulate matter and VOC emissions due to the traffic intensification. This fact is sustained by the car number counting in 10 min for each measuring point. Anova statistical approach followed by Tukey's post hoc test shows significant differences regarding legal thresholds of $PM_{2.5}$ and $PM_{10,}$ but severe excess is observed for P1, P2, P3, and P10 measuring points. There were also observed statistical differences regarding VOC values reported to the legal threshold for points P1, P2, P3, P4, and P8, with a similar situation for CO_2 for points P1, P2, P6, and P10.

Values measured at P3 and P10 points in September are almost double the level in May. Polluting conditions in both campaigns generate important levels of atmospheric particulate matter mixed up with VOC compounds. These two categories might interact, and some of the organic matter could be adsorbed onto the suspended particles, increasing their health risk. Data in the literature evidence cases of such mixed contamination [41,42].

PM_{10} variation measured with AQMS during September 2019 is presented in Figure 3. The specific values are as follows: mean value 15.46 μg/m^3; minimum 5.72 μg/m^3; maximum 51.97 μg/m^3; and daily value for 30 September 2019 is 21.62 μg/m^3. These values are significantly greater than the ones reported in May 2019, supporting our observations.

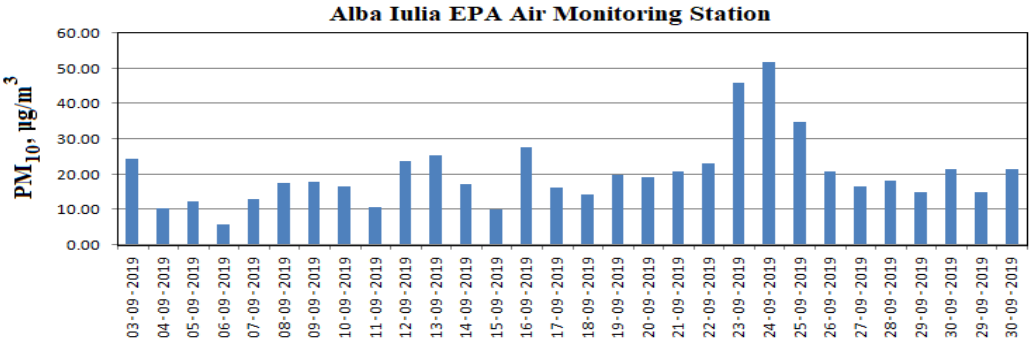

Figure 3. PM_{10} level variation during September 2019, according to Alba Iulia Environmental Protection Agency, was measured with the automated Air Quality Monitoring Station.

The emission pattern is also observed for September 2019 AQMS data. Both Monday and Friday have significantly increased values due to the traffic conditions. A single legal threshold excess (51.97 μg/m^3) was reported on 24 September 2019 (Tuesday), situated on the high level measured on 23 and 25 September 2019 due to the meteorological conditions, such as fog, associated with low aerodynamic movements. The weather ameliorates due to moderate air currents prior to our measurement preventing fog persistence. Thus, the increased values at the measuring points in our research are caused by the auto vehicle traffic.

The simplest method for pollution reduction would be traffic restriction hence the pollutant emission depends on the traffic intensity. It works only in theory because the traffic is generated by domestic, economic, and industrial needs and cannot be restricted due to the severe perturbation of all involved activities. Some of the heavy traffic might be redirected, but it will redistribute the pollution to other points. Therefore, it is difficult to figure out proper pollution-diminishing strategies based only on the measured values. A complex physicochemical investigation is required for assessing the mineral and organic compounds involved in the measured $PM_{2.5}$ and PM_{10}.

3.2. Mineral Compound Assesment

The most important investigation method for crystallized compounds and phase identification is X-ray diffraction. All collected samples were investigated, and the obtained patterns are presented in Figure 4.

All recorded XRD patterns present well-developed peaks with narrow allure and significant intensities that indicate an increased crystallinity level of the samples and a complex mixture of different minerals mixed together.

SD1 sample has the dominant peak for Quartz, Figure 4a, followed by the clay particles (such as Kaolinite and Muscovite) and calcite that originates in decayed soils from the neglected green spaces around the streets. Lepidocrocite found in the SD1 sample indicates an anthropogenic source in the rust from the car chassis. The literature data indicates that rust from the car chassis is being incorporated into the street dust [11].

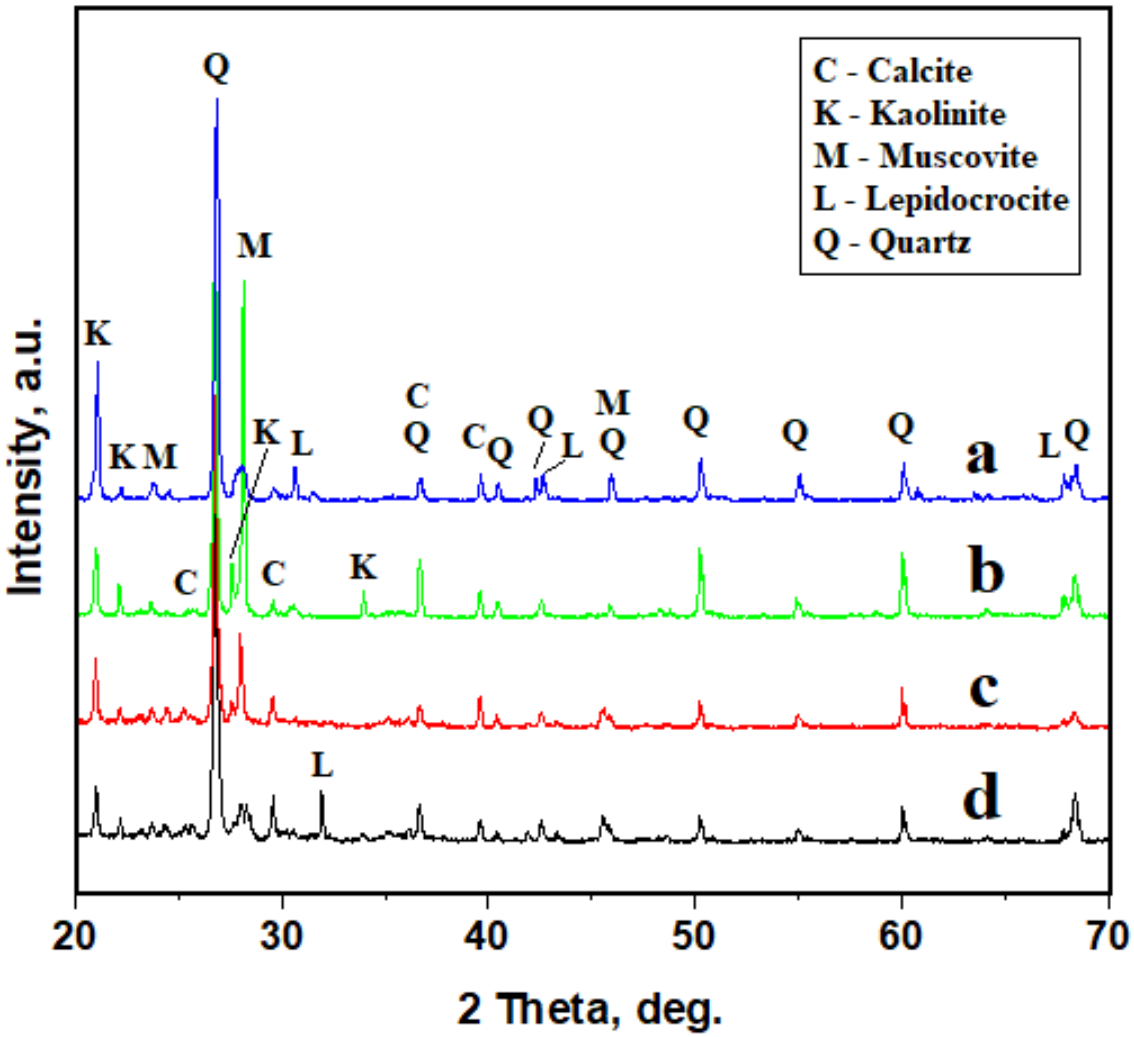

Figure 4. The XRD patterns for investigated samples: (**a**) SD1; (**b**) SD2; (**c**) ASP1; and (**d**) ASP2.

SD2 sample evidences very intense peaks, one for Quartz and the other for Muscovite, Figure 4b. Both minerals are characteristic of friable sandy clay soil that allows easy spreading of the particles into the surrounding environment if it is not properly wetted. Thus, most of the SD2 street dust sample particles originate in the neglected adjacent green spaces. XRD pattern in Figure 4b also features significant peaks for Kaolinite, Calcite, and Lepidocrocite that indicate a complex mixture of minerals tumbled together by the car's wheels.

Diffraction patterns obtained for the air-suspended particle samples, ASP1 and ASP2, Figure 4c,d have a similar aspect regarding peak positions and mineral distribution; only some minor variation of the relative intensities varies. Thus, Quartz is the dominant mineral in the ASP samples, followed by the clay mixture of Muscovite and Calcite. It represents direct proof that the decayed soil is incorporated into the street dust, and its particles are suspended in the atmosphere due to the traffic conditions. Particle size plays an important role in their atmospheric suspension, and, therefore, mineralogical microscopy is required to realize a direct connection between XRD results and particulate matter shapes and sizes.

The relative intensities of the most relevant peak of each of the identified minerals correlated with the corundum factor allow a proper determination of their weight percentage in the sample. All XRD patterns in Figure 4 were analyzed, and the resulting composition was centralized in Table 4.

Table 4. Minerals distribution within investigated samples as results of XRD and MOM investigation.

Component	Quartz	Kaolinite	Muscovite	Calcite	Lepidocrocite
Formula	SiO_2	$Al_2Si_2O_5(OH)_4$	$KAl_2(AlSi_3O_{10})(F,OH)_2$	$CaCO_3$	γFeO(OH)
Color nuances	Green–gray	White–blue	Pink	Yellow–brown	Reddish–brown
			SD1		
Amount, wt. %	36	24	19	15	6
Particle size, µm	2–160	1–55	1–30	5–80	3–15
			SD2		
Amount, wt. %	29	18	27	16	10
Particle size, µm	2–180	1–60	1–40	3–75	3–15
			ASP1		
Amount, wt. %	39	19	16	21	5
Particle size, µm	1.5–45	1–30	1–25	2–35	3–15
			ASP2		
Amount, wt. %	32	21	24	11	12
Particle size, µm	1.5–50	1–20	1–25	1.8–15	3–15

Figure 5 presents the main visual characteristics observed under cross-polarized light for the minerals identified in street dust and floating particle samples. Each of the minerals evidenced in Figure 5 was found in the investigated samples. Calcite has a boulder shape and brown–yellow nuances (Figure 5a) and evidenced dark spots on its surface when it is stained with soot (Figure 5b).

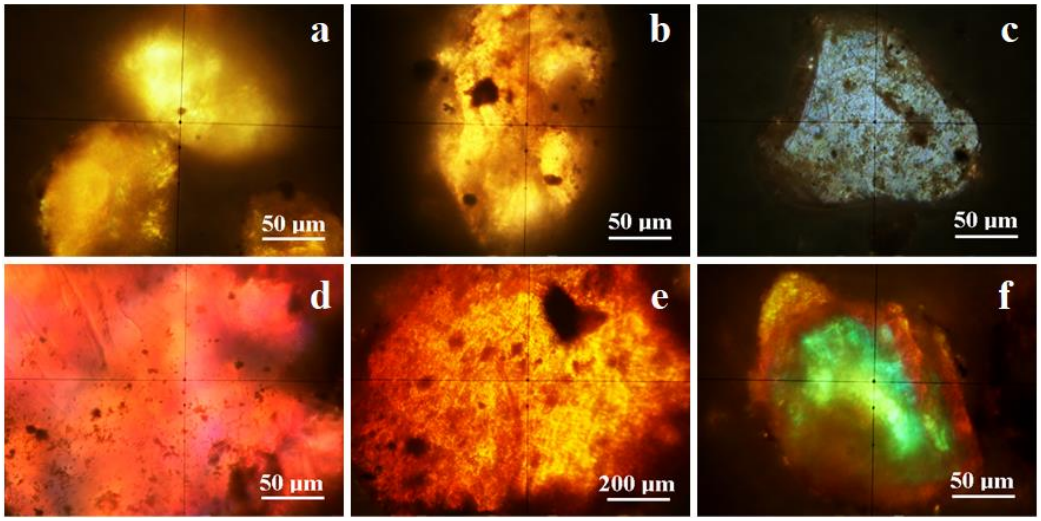

Figure 5. Cross polarized light images of the representative minerals found in SD and ASP samples: (**a**) Calcite; (**b**) Calcite with soot stains; (**c**) Kaolinite; (**d**) Muscovite; (**e**) Lepidocrocite; and (**f**) Quartz.

Kaolinite has a blue–white nuance (Figure 5c); the intense blue shade is characteristic at complete light extinction, and white nuance is observed at maximum illumination. Muscovite particles present pink shades and their intensity varies on the particle position regarding the optical axe of the microscope (Figure 5d). Lepidocrocite is an iron hydroxide, and the specific color nuance is based on red–orange shade, as observed in Figure 5e; there is observed a part of a macroscopic particle that is related to the cars rust. Several dark spots appear on its surface that belong to an amorphous material that could be of organic nature. Quartz particles normally exhibit green–gray nuance but taking into consideration the intense level of pollution within the street dust samples, they appear with an intense green shade on their top, Figure 5f.

Street dust sample SD1 has a grainy structure and a heterogeneous composition, as observed in Figure 6a. The MOM image is dominated by bigger micro-scaled particles, such as quartz and calcite, which are surrounded by the finest fractions that contain

predominantly clay particles, such as Muscovite and Kaolinite. There also appear some small particles (e.g., 2–10 μm) with green–gray shade and several sharp edges intersected under a small angle that indicates a pronounced fragmentation of Quartz.

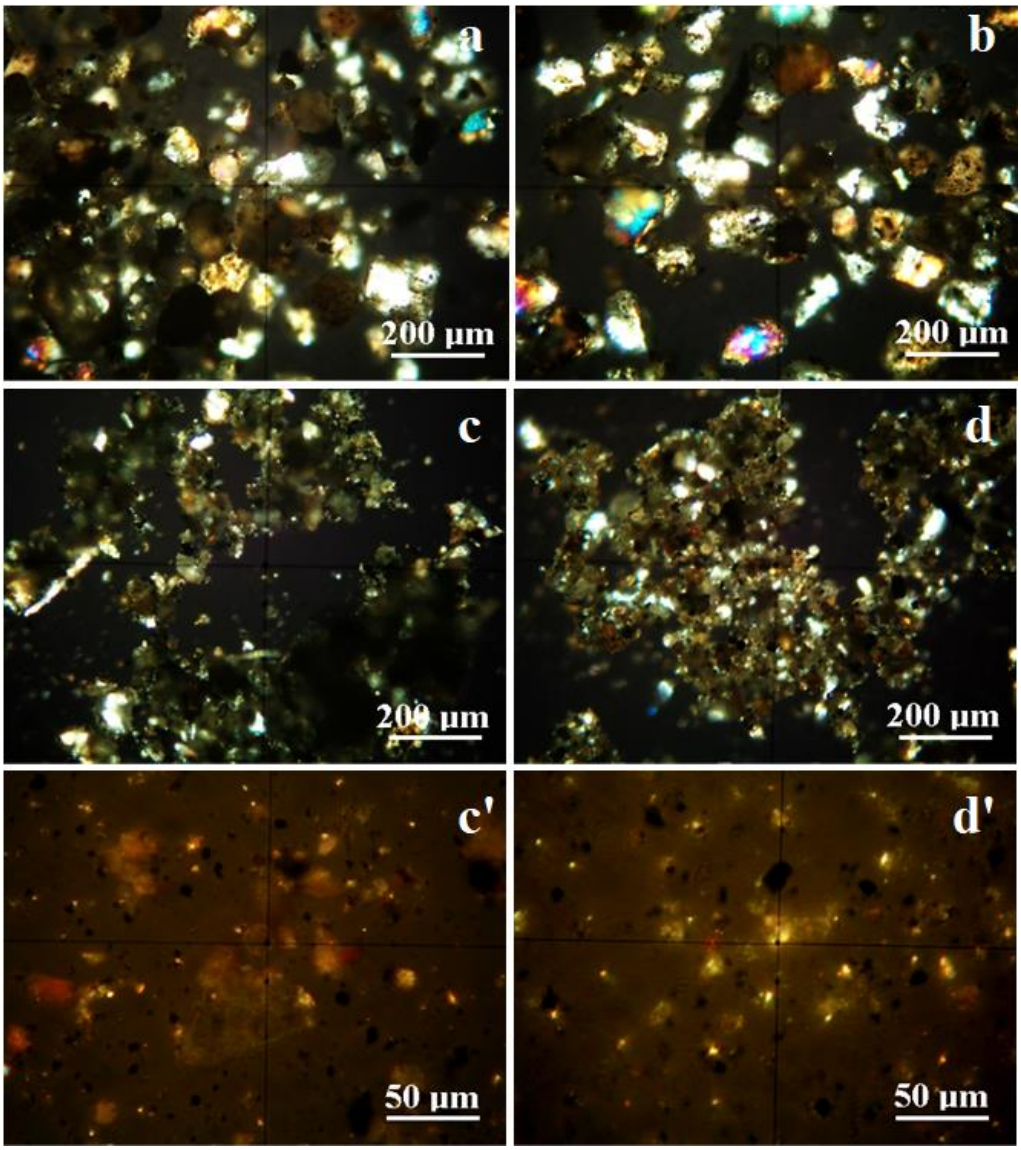

Figure 6. Cross-polarized light images of the particulate matter samples: (**a**) SD1; (**b**) SD2; (**c**) ASP1; (**d**) ASP2; (**c′**) fine fractions of ASP1; and (**d′**) fine fractions of ASP2.

It sustains the silicate fragmentation process under intensive milling induced by the vehicles' tires [32]. MOM investigation allows the proper correlation between visualized particles and XRD data, and thus, the size range is precisely established for each of the minerals, with values centralized in Table 4. Some of the bigger particles observed in the SD1 sample present dark spots that represent amorphous matter which is highly possible to be of organic nature.

SD2 sample also presents a grainy aspect with well-individualized particles in a wide range of sizes. The larger particles evidenced in Figure 6b are Quartz of about 180 μm and calcite of about 75 μm, which are surrounded by finer fractions that contain predominantly clay particles in the range of 1–60 μm but also a significant amount of fine Lepidocrocite in the range of 3–15 μm (Table 4). These fine fractions are very susceptible to being elevated into the atmosphere even by the slowest air currents. Some small black particles

are also observed, along with the finest fractions that indicate the presence of granular amorphous material.

Air-suspended particle samples that were collected from the atmosphere during May–September 2019 are very similar regarding particle size range and mineral composition, as observed in Figure 6c,d. The dominant mineral is Quartz, with particles ranging from 1.5 to 50 μm, followed by the clay particle mixture, which is preponderantly fine to ultrafine; however, their range is situated between 1 to 30 μm. It is relatively scarce in calcite presence among floating particles, but still significant content was observed in the range of 2–35 μm.

These entire minerals originated from the soil disintegration under road traffic and have dimensional components able to generate $PM_{2.5}$ and PM_{10}. Lepidocrocite proves to be the anthropogenic marker of the street dust samples SD1 and SD2 fine fractions incorporation into the ASP1 and, respectively, ASP2 because it keeps the same weight percentage from the source.

The finest fraction within the air-suspended particle samples was investigated by MOM at high magnification (Figure 6c',d'). There can be observed the particulate characteristics of $PM_{2.5}$ and PM_{10}. Both of the samples reveal that Quartz and Calcite form predominantly PM_{10}, while Muscovite and Kaolinite are predominantly situated in $PM_{2.5}$ ranges along with Lepidocrocite.

Figure 6c',d' clearly reveals some black particles with rounded shapes and sizes predominantly situated in the $PM_{2.5}$ range, but there are some bigger clusters formed by the coalescence of these particles that are situated in the PM_{10} category. These fractions need special attention because they are amorphous (the black shade of the particles observed in cross-polarized light indicates very low crystallinity or amorphous state) and are not detected by the XRD investigation. The literature data mention soot emissions associated with exhausting vehicle combustion gases [43,44].

Soot formation in combustion gases is a complex process that implies many variables, such as fuel quality, burning temperature and pressure, and environmental oxygen concentration [45]. Generally, older vehicles have combustion problems due to engine wear and lack of catalysts on the exhausting system. Diesel engines are more susceptible to forming soot due to the combustion particularities and extra lubricant requirements. Arora et al. show that initially, soot particles are nanostructured, having about 80–100 nm when generating their exact diameter depending on the Diesel working regime, a fact evidenced by TEM microscopy [46]. On the other hand, carbon nanoparticles feature a high affinity each to another, favoring their coalescence in generating bigger particles [47,48]. Finally, they drop on the soil surface, being incorporated in street dust, where they are milled together with the mineral particles. This fact is proved by the amorphous stains observed on the Calcite particle in Figure 5b and on the Lepidocrocite particle in Figure 5e. Soot particle release into the atmosphere might be correlated with the VOC values that were measured, but a more enhanced analysis is required to fulfill this allegation.

Sample morphology was investigated with Scanning Electron Microscopy (SEM) for a better observation of the particle morphology and sizes using magnifications and resolution better than MOM. Bigger street dust particles found in SD1 and SD2 samples were first investigated (Figure 7).

Bigger particles of street dust are practically inevitable in the conditions of a big city with complex socio-economical activities. These particles are visible to the eyes without any magnifying device because of their sizes close to 1 mm. They are not susceptible to being lifted into the atmosphere but could play an important role in the particulate matter pollution mechanism.

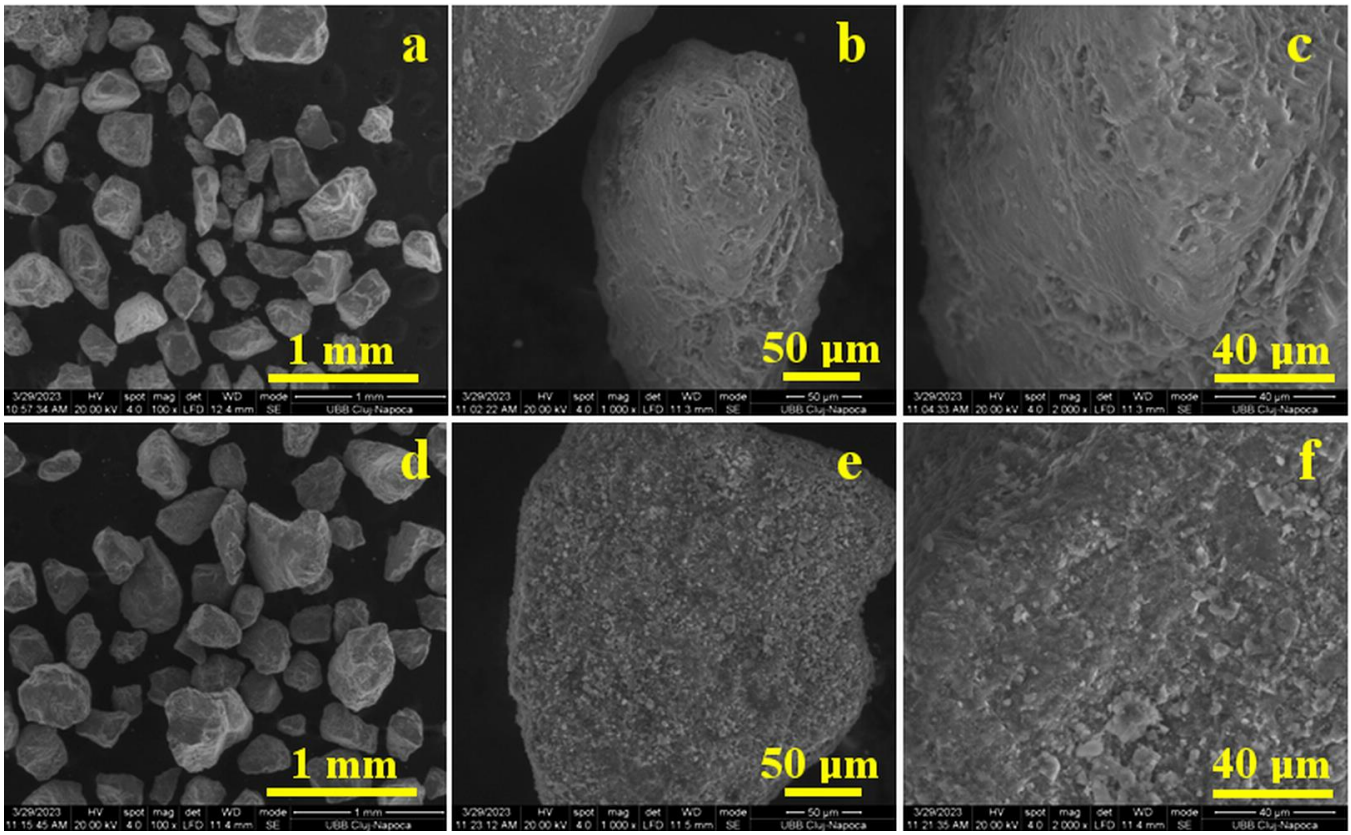

Figure 7. SEM images for large particles within street dust samples SD1: (**a**) macroscopic detail; (**b**) single particle view; and (**c**) microstructural details. SD2: (**d**) macroscopic detail; (**e**) single particle view; and (**f**) microstructural details.

For example, SD1's bigger particles' general aspect is observed in the SEM image presented in Figure 7a. Their sizes range from 500–800 µm and look as freshly-broken quartz particles due to the sharp edges intersecting on small angles. This fact is in good agreement with the silicate fragmentation mechanism [32]. The freshly broken quartz particles apparently disagree with the MOM observation, where the Quartz particles appear to be covered with pollutants. Therefore, a closer look at one of the bigger particles (Figure 7b) allows observing its irregular surface with a lot of the finest fractions embedded into some kind of coating. The examination at high magnification (Figure 7c) evidences a lot of small lamellar particles belonging to clays with dimensions predominantly found in the $PM_{2.5}$ ranges. This fact explains the reddish color ring around the green top of the quartz particle exemplified in Figure 3f. The embedding binder might be soot generated by an old vehicle combustion exhausting system.

A similar aspect is observed for the SD2 sample featuring bigger Quartz particles with blunted edges as a consequence of intensive mechanical stress involved in their interaction between them and cars' tires (Figure 7d). The detail on SD2 bigger particle evidences better the finest particles coating on its surface (Figure 7e,f). There appear to be few evident PM_{10} particles that are surrounded by a lot of fine particles in the range of $PM_{2.5}$. Some of them are small enough to be categorized as PM_1 fractions.

Microstructured fractions of the SD1 sample are observed by SEM microscopy in Figure 8a, revealing a heterogeneous mixture with the aspect of intensive milling of the mineral particles.

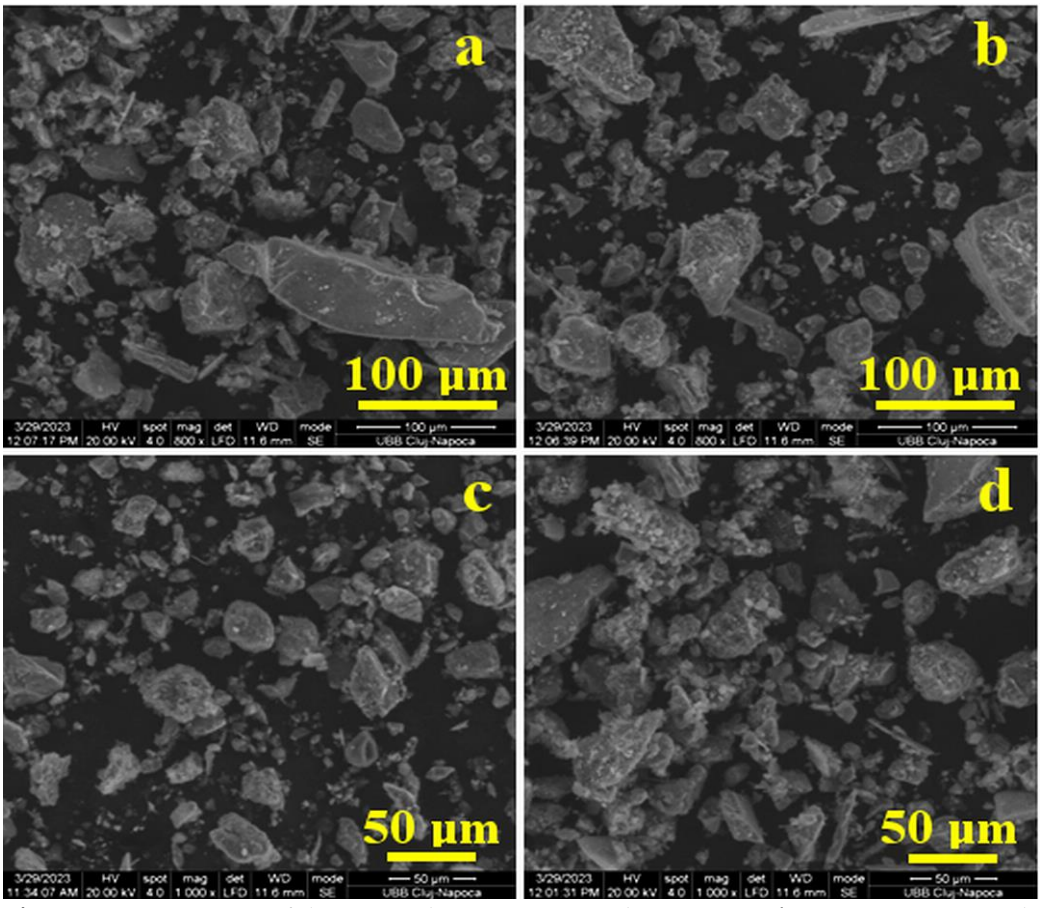

Figure 8. SEM images of the particulate matter samples: (**a**) SD1; (**b**) SD2; (**c**) ASP1; and (**d**) ASP2.

The right side of Figure 8a evidence a fresh quartz sliver having a length of 150 µm and a width of about 60 µm and presents a few small clay particles adsorbed on its surface, while the upper right corner evidences a rounded calcite particle of about 40 µm and a quartz fragment with a sharp arrow tip of about 42 µm. These features are surrounded by a lot of fine Quartz and Calcite particles situated in the PM_{10} size range and a lot of finer clay particles in size range corresponding to $PM_{2.5}$. Similar aspects regarding $PM_{2.5}$ and PM_{10} particulate fractions are observed for the SD2 sample (Figure 8b); the differences consist of two quartz particles with dimensions over 100 µm that are fully covered with finest fractions, as observed in the upper left corner and on the right side of the images' observation field.

Air-suspended particle sample ASP1 was investigated with SEM microscopy, and the resulting image is presented in Figure 8c and assures a better visual quality than the complementary MOM image in Figure 6c' (both images have the same scale bar). Particles situated in the range of 11–45 µm belong predominantly to quartz and calcite. These sizes exceed the particulate matter standard, but they also were lifted into the atmosphere by the intense auto vehicle traffic, but their suspension time was slightly shorter than the other finest fractions. Figure 8c reveals that the PM_{10} fraction contains predominantly Quartz and Calcite, and $PM_{2.5}$ contains predominantly Kaolinite and Muscovite particles. It consists of solid proof that mineral particulate matter within the ASP1 sample originates in the SD1 street dust.

The ASP2 sample was also investigated by SEM microscopy (Figure 8d) in order to assure a better morphological view than the MOM observation in Figure 6d'. There appear some quartz particles of about 50 µm (in good agreement with MOM investigation) with sharp edges and small fraction, adsorbed on their surfaces. The other particles in the range of 11–30 µm belonged both to quartz and calcite and were lifted into the atmosphere by the

intensive car traffic along with the particulate matter. Mineral distribution within $PM_{2.5}$ and PM_{10} categories is similar to the one observed for ASP1, but the intensive fragmentation of the clay particles, which predominates into the $PM_{2.5}$, is more evident in Figure 6d, and a lot of those particles are eligible to be categorized as PM_1. However, this class is included in $PM_{2.5}$ and is not treated as a separate category since there are no legal provisions and devices for their level measurement as distinct indicators.

The mineral compounds assessment concludes that street dust is a main source of particulate matter in the atmosphere due to intensive vehicle traffic. Their tires act over the dust particles as a mill and the bigger quartz particles as milling bodies. Therefore, clay particles are more brittle and are fragmented until a lot of the finest fractions are formed. These are enclosed in the $PM_{2.5}$ fraction. Calcite and some of the Quartz particles are fragmented during the milling process until they reach small sizes, but they are found predominantly in PM_{10} and less in the $PM_{2.5}$ category.

In consequence, mineral particulate matter mitigation might be implemented by a more enhanced street cleaning using dust collectors and do not require traffic limitations. The measure would be more powerful if the street dust sources were reduced. Therefore, supplementary care of the green areas would reduce the street dust occurrence.

3.3. Organic Compound Assessment

The first step of the organic matter assessment was conducted with an FTIR investigation. Street dust and air-suspended particle samples were investigated, and the obtained spectra are presented in Figure 9. This spectroscopic investigation reveals the vibration bands of each chemical bond in the sample compounds, which appear at specific wave numbers. Therefore, each evidenced absorption band was compared with the database and the literature for the proper vibrations assignment; all measured peaks were centralized in Table 5, and on their right side is presented the proper assignment according to the cited literature.

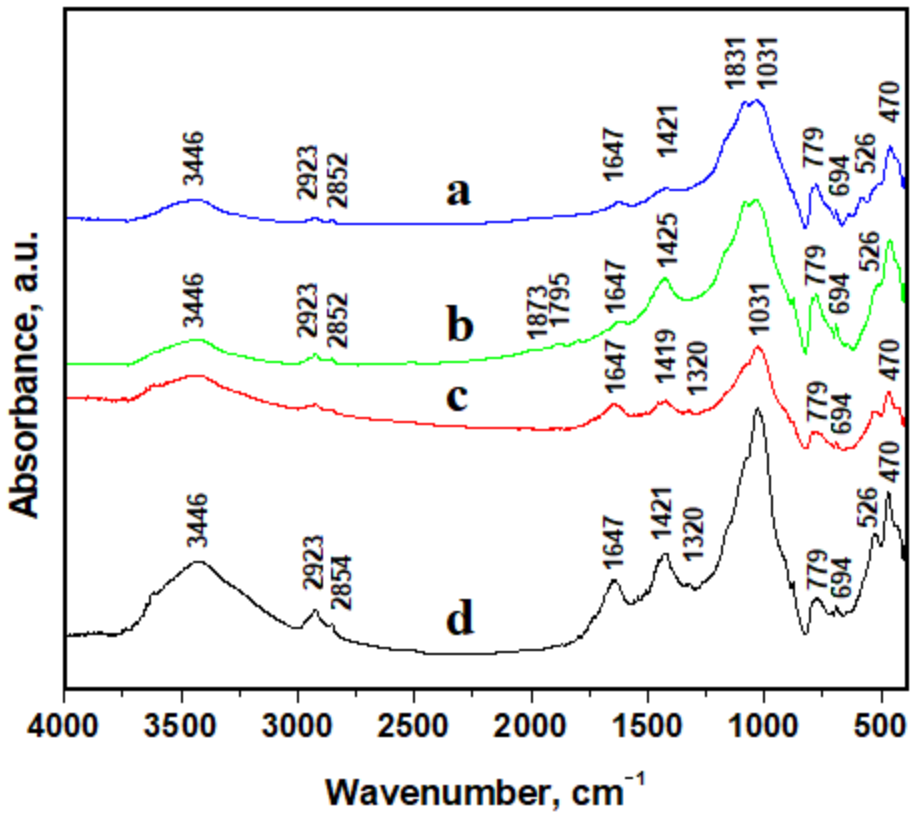

Figure 9. FTIR spectra for investigated samples: a—SD1; b—SD2; c—ASP1; and d—ASP2.

Table 5. FTIR absorption band assignment.

Species	Measured Peak Wavenumber (cm^{-1})				Vibrations Assignment	References
	ASP1	ASP2	PS1	PS2		
Water (OH)	3431	3431	3446	3421	H-O-H stretching	[49,50]
	1626	1620			H-O-H bending	
C-H (alkanes)	2923	2923	2923	2923	$-CH_2$ asymmetric stretching	[50]
	2852	2852	2854	2854	$-CH_2$ Symmetric stretching	
C=O (organic compounds)	1873	1870			Saturated symmetric C=O stretch	[49]
			1647	1676	C=O stretch	
CO_3^{2-} (calcium carbonate)	1795	1797			CO_3^{2-} ions	[51]
NH_4^+	1421	1425	1419	1421	NH_4^+ ions	[52]
NO_3^-			1320	1320	NO^-_3 ions	[50,53]
SO_4^{2-}	1081	1080			S-O stretch	[52,53]
	638	646			S-O bend	
Silicates	1035	1035	1039	1029	in-plane Si-O stretching	
	777	777	779	777	Si-O-Si vibration	[50]
	694	694	694	692	Si-O symmetrical bending	
	582				O-Si-O bending deformation	[54]
	511	512	526	526		
	460	461	470	468	O-Si-O bending deformation	

All samples contain adsorbed water evidenced by H-O-H stretching at 3421–3431 cm^{-1} and H-O-H bending evidenced at 1620–1626 cm^{-1} only in SD1 and SD2 samples, which is in good agreement with the literature [49,50]. It proves that floating particles contain less adsorbed water than street dust.

Organic matter proves to be strongly represented by alkanes and their $-CH_2$ asymmetric stretching evidenced at 2923 cm^{-1} and $-CH_2$ Symmetric stretching at 2852–2584 cm^{-1}. The other organic compounds categories evidence C=O bounds as saturated symmetric C=O stretch at 1870–1873 cm^{-1} for street dust samples and C=O stretch at 1647–1676 cm^{-1} for the floating particle samples. The C=O absorption band difference between street dust and floating particles might be explained by the fresh interaction of the floating particles with combustion gases, and, thus, some organic volatile compounds might be adsorbed on their surface. On the other hand, street dust samples contain a significant amount of amorphous matter that is related to the soot clusters bonded together by the other C=O organic compounds evidenced by FTIR analysis.

Mineral fractions within street dust and floating particle samples are strongly represented by the CO_3^{2-} ions absorption band at 1795–1797 in close relation with calcite and silicates absorption bands related to the Quartz, Muscovite, and Kaolinite. These are as follows: in-plane Si-O stretching at 1029–1035 cm^{-1}; Si-O-Si vibration at 777–779 cm^{-1}; Si-O symmetrical bending at 692–694 cm^{-1}; O-Si-O bending deformation at 511–526 cm^{-1}; and O-Si-O bending deformation at 460–468 cm^{-1}. It is very interesting that species, such as NH_4^+; NO_3^-, and SO_4^{2-}, are evidenced by the absorption bands of 1421 cm^{-1}; 1320 cm^{-1}, and 1080 cm^{-1}. These might be related to the derivative sub-product of SO_2 and NO_2 emissions into the atmosphere, which is related to the acid rain compounds [20]. Ammonia chemical bonds were found both in street dust samples and in air-suspended particle samples, while sulfate chemical bonds were observed only in street dust.

A significant amount of VOC measured during May and September 2019 is expected to influence particulate matter emissions. Some of these compounds might be adsorbed on the mineral and soot particles, increasing their hazardous potential. This fact was proved by the gas chromatography and mass spectrometry GC-MS analysis effectuated on ASP1 and ASP2 samples. The obtained TIC chromatograms are presented in Figure 10, and the relevant peaks are marked with their retention time (RT).

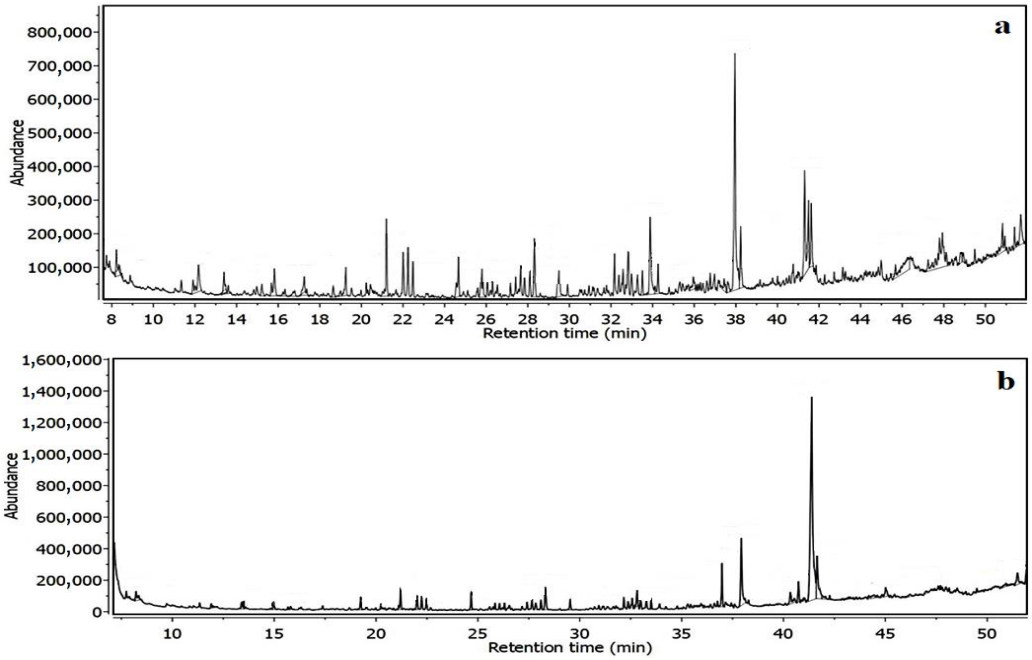

Figure 10. TIC chromatograms for investigated samples: (**a**) ASP1; and (**b**) ASP2.

TIC chromatograms were processed by the soft instrument, and the total composition of volatile compounds extracted from ASP1 and ASP2 samples was obtained. The results are centralized in Table 6: each of the identified compounds is listed according to the retention time (RT), and its weight percent is presented.

Table 6. Volatile Organic Compounds identified by GC-MS analysis in ASP1 and ASP2 samples.

No	Compound	RT, min.	VOC, %		No	Compound	RT, min.	VOC, %	
			ASP1	ASP2				ASP1	ASP2
1	Toluene	7.747	0.56	0.52	28.	Undecanoic acid, ethyl ester	29.913	0.50	-
2.	2-Hexanone	8.223	1.31	1.05	29.	Cyclohexane,1,1,3,5-tetramethyl	32.165	2.42	1.14
3.	2-Hexene-1-methoxy	8.349	0.49	0.57	30.	Cyclohexane,1,2-diethyl-3-methyl	32.577	1.52	1.01
4.	Ethane1,1,2,2-tetrachloro	12.168	2.73	-	31.	Cyclooctane,1-methyl-3-propyl	32.815	3.67	2.57
5.	Butyl angelate, 3-methyl	13.399	2.05	1.05	32.	Octacosylheptafluorobutyrate	33.271	1.29	1.12
6.	D-Limonene	14.966	0.69	0.66	33.	Tetradecanoic acid	33.885	5.93	-
7.	Pentanoic acid, 2-propenyl ester	15.217	1.00	-	34.	Octadecane	33.919	-	0.63
8.	Pentanoic acid, ethylhexyl ester	15.816	1.91	-	35.	Tetradecanoic acid, ethyl ester	34.264	1.53	-
9.	2-methyl-6-methyleneocta-2,4-dienone	17.255	1.76	-	36.	Nonadecane	35.956	0.34	-
10.	10-chloro-1-decanol	18.642	0.84	-	37.	Hexadecanoic acid, methyl ester	36.983	1.13	3.71
11.	Undecane	19.247	2.00	1.27	38.	Hexadecanoic acid	37.958	19.86	9.21
12.	Undecane,4,6-dimethyl	20.234	0.56	0.21	39.	Hexadecanoic acid, ethyl ester	38.229	3.28	-
13.	Decane,2,3,5,8-tetramethyl	20.438	0.76	-	40.	Z,Z-3,13-Octadien-1-ol	40.347	-	1.87
14.	1.3-Di-tert-butylbenzene	21.205	3.91	1.81	41.	Methyl stearate	40.738	-	2.41
15.	Undecane-3,7-dimethyl	22.003	3.04	1.57	42.	Z-9-octadecenoic acid	41.306	6.34	44.51
16.	Cyclohexane, 1,2,4-trimethyl	22.244	2.81	1.30	43.	Octadecanoic acid	41.627	4.20	5.66
17.	Cyclopentane, 2-methylbutyl	22.476	2.11	1.12	44.	Ethyl tridecanoate	41.859	0.51	-
18.	n-decanoic acid	24.569	0.53	-	45.	Tricosan	43.274	0.44	-
19.	Tetradecane	24.670	1.63	1.48	46.	Pentadecane, 2,6,10,14-tetramethyl	45.012	1.06	1.78
20.	Dodecane,2,6,10-trimethyl	25.587	0.71	-	47.	Z-9- octadecenoic acid, pentyl ester	45.678	0.50	-
21.	2,6,10-trimethyltridecane	26.060	0.89	0.71	48.	Bis(2-ethylhexyl)phtalate	47.719	0.29	0.70
22.	Pentadecane	27.166	0.66	0.38	49.	Decyloleate	47.796	0.98	-
23.	Cyclopentane (2-methylbutyl)	27.655	-	1.14	50.	Pentadecene	47.930	1.83	1.18
24.	Cyclohexane,1-ethyl-2-propyl	28.098	1.52	0.95	51.	Heptacosan	49.491	0.66	0.4
25.	2,4-Di-tert-butylphenol	28.312	4.16	2.98	52.	Squalene	51.398	0.93	-
26.	Dodecanoic acid	29.445	1.00	-	53.	E-9-octadecenoic acid, pentyl ester	51.483	-	1.96
27.	Hexadecane	29.531	0.70	1.18	Total			99.54	99.81

Results show with no doubt that air-suspended particles retain a lot of the VOCs resulting from the combustion gases. Saturated alkanes, cycloalkanes, fat acid, and fatty acid esters were dominant compounds in good agreement with the data in the literature [55,56]. Kim and Koh divided the VOC identified in the street dust into four groups, such as

aliphatic hydrocarbons, phenol derivatives, aromatic hydrocarbons, and oxidized hydrocarbons [55]. The amount of VOC allows for establishing emission patterning, according to the sample source. However, in our case, it is sufficient that VOCs' presence in the air-suspended particle samples is sufficient as a first point of view.

Moreover, the literature data relates the saturated alkanes to the combustion gasses residues, especially from diesel fuels which are further incorporated into the soot particles [57,58]. This observation deals with the Diesel combustion type, which requires supplementary lubrication of the fuel, a fact that facilitates soot formation and incorporation of the volatile compounds in its particles. Diesel fuel also contains significant aromatic hydrocarbons that generate specific VOCs after combustion [59]. Such aromatic compounds were identified in ASP1 and ASP2, such as toluene, 1.3-Di-tert-butylbenzene, and Bis(2-ethylhexyl)phthalate, which are hazardous for the health, which is in good agreement with the data in the literature [60].

The most efficient soot mitigation strategy and combustion-related VOCs are using modern catalyst systems and advanced filters installed on the exhausts. These devices convert dangerous VOCs to less hazardous compounds and retain associated particle emissions.

3.4. Study Limitations and Future Prospective

The complexity of the present research is given by the correlation established between PM emissions measured directly on the street at the most polluted points in Alba Iulia and their generation mechanism caused by vehicle traffic.

The most intriguing aspect is the apparent discrepancy between the PM level measured directly on the street and the values measured by the Automated Air Quality Monitoring station. Our measurement shows limit threshold excess for almost investigated points during May and for all measuring points during September, while AQMS evidences only mild excess of PM_{10} during September. It means that the high level of pollutant measured directly at the source is partially dissipated until reaching the AQMS, but it also means that PM pollution issues are strictly limited at most intense traffic nodes, and it is not propagated in the whole city. Therefore, one of the main limitations of this study is given the reduced number of direct observations in the street, a fact which should be improved during future research.

Physicochemical investigations evidence that street dust causes significant particulate matter emissions due to the intense traffic and air current intensity, which causes particle suspension into the atmosphere. These air-suspended particles are very heterogeneous, containing mineral and organic fractions. ASP mineral fractions, such as Quartz, Calcite, Muscovite, Kaolinite, and Lepidocrocite, are generated by street dust, while organic fractions are mostly soot resulting from vehicle combustion. Mineralogical optical microscopy allows proper dimensional classification of the observed PMs. Therefore, Quartz and Calcite are predominantly found in the PM_{10} fraction category, and the $PM_{2.5}$ fraction contains predominantly Muscovite and Kaolinite. Thus, the investigation of street dust and air-suspended particles from the P3 and P10 measuring points is another limitation of the present research. It requires more samples to be collected and investigated in the future in order to establish a proper mitigation strategy.

Soot microparticles are formed by their nanoparticles clustering in the presence of combustion VOCs. Therefore, some volatile organic compounds might be retained in such clusters. GC-MS analysis evidenced 53 different VOCs belonging to different classes, such as aromatic hydrocarbons, alkanes, cycloalkanes, complex alcohols, and ketones. All these VOCs were extracted from the ASP samples, and their presence proves that their hazardous potential is increasing. Unfortunately, a limitation of this study is that atmospheric VOC emission measurements allowed us to establish the value of total emitted VOCs but didn't allow their individual speciation to be compared with GC-MS data obtained for ASP samples. The further approach to this issue requires more enhanced measuring devices for the proper detection of certain individual VOCs.

The mitigation of PM emission into the atmosphere strategy identified in the obtained results implies better care of the street adjacent green fields to avoid their decaying for a drastic limitation of mineral particles occurrence in the street. Another useful strategy is the implementation of advanced filters for all vehicles to reduce soot and VOC emissions.

4. Conclusions

The atmospheric parameter measuring campaigns effectuated in Alba Iulia in May and September 2019 revealed a significant excess of particulate matter pollution associated with a significant amount of VOC and CO_2 emissions caused by intensive vehicle traffic.

Physicochemical investigations reveal that air-suspended particles, including $PM_{2.5}$ and $PM_{10,}$ contain significant amounts of mineral fractions originating in the street dust and organic particles of soot. These results show that PM_{10} fractions contain predominantly Quartz and Calcite and traces of clay particles, and $PM_{2.5}$ fractions contain predominantly Muscovite and Kaolinite particles and traces of Quartz, Calcite, and Lepidocrocite.

Soot particles are found as small micron clusters that proliferate mainly into the $PM_{2.5}$ category, but some of them are found in PM_{10}. The presence of soot and its related VOCs was confirmed by the CH_2 and C=O bonds, evidenced by FTIR spectroscopy. GC-MS investigation proves that the combustion gases related to VOCs are retained by the particulate matter, increasing their hazardous potential.

The results indicated that the most efficient particulate matter mitigation strategy is to reduce street dust occurrence by better care of the street-adjacent green areas and an enhanced street cleaning program. The organic compounds and soot mitigation strategy is the implementation of modern filters and catalytic systems on the vehicle combustion gases exhausting systems. Another VOCs' mitigation strategy would be the replacement of the oldest combustion vehicles with new electrical ones.

Author Contributions: Conceptualization, M.R. and T.R.; methodology, S.E.A. and I.P.; software, T.A.R. and P.P.; validation, T.R., I.P. and S.E.A.; formal analysis, G.A.P. and M.R.; investigation, M.R., S.E.A., D.P., M.R.F., I.C., P.P., I.P. and T.A.R.; resources, T.R.; data curation, G.A.P., S.E.A.; writing—original draft preparation, G.A.P. and I.P.; writing—review and editing, G.A.P. and I.P.; visualization, D.P. and I.P.; supervision, I.P. and T.R.; project administration, T.R.; funding acquisition, M.R. and T.R. All authors have read and agreed to the published version of the manuscript.

Funding: The APC was supported by Technical University of Cluj-Napoca through application No. 14428/11.05.2023.

Institutional Review Board Statement: Not applicable.

Informed Consent Statement: Not applicable.

Data Availability Statement: Data are available on request from the corresponding author.

Acknowledgments: The authors of the present article gratefully acknowledge the Environmental Protection Agency in Alba Iulia, Romania, for PM_{10} values measured with the Automated Air Quality Measuring Station during May and September 2019.

Conflicts of Interest: The authors declare no conflict of interest.

References

1. Ferm, M.; Sjöberg, K. Concentrations and emission factors for $PM_{2.5}$ and PM_{10} from road traffic in Sweden. *Atmos. Environ.* **2015**, *119*, 211–219. [CrossRef]
2. Zhang, Q.; Sun, L.; Wei, N.; Wu, L.; Mao, H. The characteristics and source analysis of VOCs emissions at roadside: Assess the impact of ethanol-gasoline implementation. *Atmos. Environ.* **2021**, *263*, 118670. [CrossRef]
3. Cachon, F.B.; Cazier, F.; Verdin, A.; Dewaele, D.; Genevray, P.; Delbende, A.; Ayi-Fanou, L.; Aïssi, F.; Sanni, A.; Courcot, D. Physicochemical Characterization of Air Pollution Particulate Matter ($PM_{2.5}$ and $PM_{>2.5}$) in an Urban Area of Cotonou, Benin. *Atmosphere* **2023**, *14*, 201. [CrossRef]
4. Petean, I.; Mocanu, A.; Păltinean, G.A.; Ţărcan, R.; Muntean, D.F.; Mureşan, L.; Arghir, G.; Tomoaia-Cotişel, M. Physico-Chemical Study Concerning Atmospheric Particulate Matter Hazard. *Stud. Univ. Babes-Bolyai Chem.* **2017**, *62*, 33–46. [CrossRef]

5. Păltinean, G.A.; Petean, I.; Arghir, G.; Muntean, D.F.; Boboş, L.D.; Tomoaia-Cotişel, M. Atmospheric Induced Nanoparticles Due to the Urban Street Dust. *Particul. Sci. Technol.* **2016**, *34*, 580–585. [CrossRef]
6. Hosu-Prack, G.A.; Petean, I.; Arghir, G.; Boboş, L.D.; Tomoaia-Cotişel, M. Nano-Scale Particulate Matters Found in Urban Street Dust in Cluj-Napoca, Romania. *Carpathian J. Earth Environ. Sci.* **2016**, *11*, 539–546.
7. Kupiainen, K.; Ritola, R.; Stojiljkovic, A.; Pirjola, L.; Malinen, A.; Niemi, J. Contribution of mineral dust sources to street side ambient and suspension PM10 samples. *Atmos. Environ.* **2016**, *147*, 178–189. [CrossRef]
8. Švédová, B.; Matýsek, D.; Raclavská, H.; Kucbel, M.; Kantor, P.; Šafář, M.; Raclavský, K. Variation of the chemical composition of street dust in a highly industrialized city in the interval of ten years. *J. Environ. Manag.* **2020**, *267*, 110506. [CrossRef]
9. Iwegbue, C.M.A.; Ehigbor, M.J.; Tesi, G.O.; Eguavoen, O.I.; Martincigh, B.S. Occurrence, Sources and Exposure Risk of Polycyclic Aromatic Hydrocarbons (PAHs) in Street Dusts from the Nigerian Megacity, Lagos. *Polycycl. Aromat. Compd.* **2022**, *42*, 49–69. [CrossRef]
10. Pang, L.; Huang, Z.; Yang, H.; Pang, R.; Wu, M.; Jin, B. A scalable field study using leaves as a novel passive air sampler to evaluate the potential source of organophosphate esters in street dust. *Chemosphere* **2023**, *312*, 137248. [CrossRef]
11. Muntean, D.F.; Ristoiu, D.; Arghir, G.; Campean, R.F.; Petean, I. Iron hydroxides occurrence in winter air particulate matters suspensions in Cluj-Napoca, Romania. *Carpathian J. Earth Environ. Sci.* **2012**, *7*, 175–182.
12. Mandal, M.; Popek, R.; Przybysz, A.; Roy, A.; Das, S.; Sarkar, A. Breathing Fresh Air in the City: Implementing Avenue Trees as a Sustainable Solution to Reduce Particulate Pollution in Urban Agglomerations. *Plants* **2023**, *12*, 1545. [CrossRef] [PubMed]
13. Kwak, M.J.; Lee, J.; Park, S.; Lim, Y.J.; Kim, H.; Jeong, S.G.; Son, J.-a.; Je, S.M.; Chang, H.; Oh, C.-Y.; et al. Understanding Particulate Matter Retention and Wash-Off during Rainfall in Relation to Leaf Traits of Urban Forest Tree Species. *Horticulturae* **2023**, *9*, 165. [CrossRef]
14. Singh, S.K.; Chowdhary, G.R.; Purohit, G. Assessment of Impact of High Particulate Concentration on Peak Expiratory Flow Rate of Lungs of Sand Stone Quarry Workers. *Int. J. Environ. Res. Public Health* **2006**, *3*, 355–359. [CrossRef] [PubMed]
15. Ramar, M.; Yano, N.; Fedulov, A.V. Intra-Airway Treatment with Synthetic Lipoxin A4 and Resolvin E2 Mitigates Neonatal Asthma Triggered by Maternal Exposure to Environmental Particles. *Int. J. Mol. Sci.* **2023**, *24*, 6145. [CrossRef]
16. Dhong, K.-R.; Lee, J.-H.; Yoon, Y.-R.; Park, H.-J. Identification of TRPC6 as a Novel Diagnostic Biomarker of PM-Induced Chronic Obstructive Pulmonary Disease Using Machine Learning Models. *Genes* **2023**, *14*, 284. [CrossRef]
17. Xia, S.-Y.; Huang, D.-S.; Jia, H.; Zhao, Y.; Li, N.; Mao, M.-Q.; Lin, H.; Li, Y.-X.; He, W.; Zhao, L. Relationship between atmospheric pollutants and risk of death caused by cardiovascular and respiratory diseases and malignant tumors in Shenyang, China, from 2013 to 2016: An ecological research. *Chin. Med. J.* **2019**, *132*, 2269–2277. [CrossRef]
18. Nirmalkar, J.; Lee, K.; Ahn, J.; Lee, J.; Song, M. Comparisons of Spatial and Temporal Variations in $PM_{2.5}$-Bound Trace Elements in Urban and Rural Areas of South Korea, and Associated Potential Health Risks. *Atmosphere* **2023**, *14*, 753. [CrossRef]
19. Święczkowski, M.; Dobrzycki, S.; Kuźma, Ł. Multi-City Analysis of the Acute Effect of Polish Smog on Cause-Specific Mortality (EP-PARTICLES Study). *Int. J. Environ. Res. Public Health* **2023**, *20*, 5566. [CrossRef]
20. Hosu-Prack, G.A.; Petean, I.; Arghir, G.; Bobos, L.D.; Iurcut, I.; Tomoaia-Cotisel, M. Marble nano erosion under acid rain evidenced by atomic force microscopy. *Carpathian J. Earth Environ. Sci.* **2013**, *8*, 75–82.
21. Wei, Y.; Li, Z.; Zhang, Y.; Li, K.; Chen, J.; Peng, Z.; Hu, Q.; Goloub, P.; Ou, Y. The Effects of Local Pollution and Transport Dust on Aerosol Properties in Typical Arid Regions of Central Asia during DAO-K Measurement. *Atmosphere* **2022**, *13*, 729. [CrossRef]
22. Fussell, J.C.; Franklin, M.; Green, D.C.; Gustafsson, M.; Harrison, R.M.; Hicks, W.; Kelly, F.J.; Kishta, F.; Miller, M.R.; Mudway, I.S.; et al. A Review of Road Traffic-Derived Non-Exhaust Particles: Emissions, Physicochemical Characteristics, Health Risks, and Mitigation Measures. *Environ. Sci. Technol.* **2022**, *56*, 6813–6835. [CrossRef]
23. Montero-Montoya, R.; López-Vargas, R.; Arellano-Aguilar, O. Volatile Organic Compounds in Air: Sources, Distribution, Exposure and Associated Illnesses in Children. *Ann. Glob. Health* **2018**, *84*, 225–238. [CrossRef] [PubMed]
24. Huang, H.; Hu, H.; Zhang, J.; Liu, X. Characteristics of volatile organic compounds from vehicle emissions through on–road test in Wuhan, China. *Environ. Res.* **2020**, *188*, 109802. [CrossRef] [PubMed]
25. Wang, H.L.; Jing, S.A.; Lou, S.R.; Hu, Q.Y.; Li, L.; Tao, S.K.; Huang, C.; Qiao, L.P.; Chen, C.H. Volatile organic compounds (VOCs) source profiles of on-road vehicle emissions in China. *Sci. Total Environ.* **2017**, *607–608*, 253–261. [CrossRef]
26. Fuller, R.; Landrigan, P.J.; Balakrishnan, K.; Bathan, G.; Bose-O'Reilly, S.; Brauer, M.; Caravanos, J.; Chiles, T.; Cohen, A.; Corra, L.; et al. Pollution and health: A progress update. *Lancet Planet Health* **2022**, *6*, e535–e547. [CrossRef]
27. Council Directive 1999/30/EC of 22 April 1999 Relating to Limit Values for Sulphur Dioxide, Nitrogen Dioxide and Oxides of Nitrogen, Particulate Matter and Lead in Ambient Air. Available online: https://eur-lex.europa.eu/legal-content/EN/TXT/?uri=CELEX%3A31999L0030&qid=1680678998848 (accessed on 5 April 2023).
28. Directive 2008/50/EC of the European Parliament and of the Council of 21 May 2008 on Ambient Air Quality and Cleaner Air for Europe. Available online: http://eur-lex.europa.eu/legal-content/en/ALL/?uri=CELEX:32008L0050 (accessed on 5 April 2023).
29. Law No. 104 of 15 June 2011 on Ambient Air Quality, Updated on 22 May 2015. Available online: https://www.global-regulation.com/translation/romania/3755838/law-no.-104-of-15-june-2011-on-ambient-air-quality.html (accessed on 5 April 2023).
30. WHO. *Global Air Quality Guidelines, Particulate Matter ($PM_{2.5}$ and PM_{10}), Ozone, Nitrogen Dioxide, Sulfur Dioxide and Carbon Monoxide*; Licence: CC BY-NC-SA 3.0 IGO; World Health Organization: Geneva, Swizterland, 2021. Available online: https://www.who.int/publications/i/item/9789240034228 (accessed on 4 April 2023).

31. Ministry of the Environment. Air Quality, National Air Quality Monitoring Network, Quality Indices. Available online: https://www.calitateaer.ro/public/monitoring-page/quality-indices-page/?__locale=ro (accessed on 5 April 2023).
32. Păltinean, G.A.; Petean, I.; Arghir, G.; Muntean, D.F.; Tomoaia-Cotişel, M. Silicates Fragmentation a Source of Atmosphere Dispersed Nano—Particulate Matter. *Rev. Chim.* **2016**, *67*, 1118–1123.
33. Zhang, M.; Sun, H.; Song, C.; Li, Y.; Hou, M. Pores Evolution of Soft Clay under Loading/Unloading Process. *Appl. Sci.* **2020**, *10*, 8468. [CrossRef]
34. Pérez-Sansalvador, J.C.; Lakouari, N.; Garcia-Diaz, J.; Hernández, S.E.P. The Effect of Speed Humps on Instantaneous Traffic Emissions. *Appl. Sci.* **2020**, *10*, 1592. [CrossRef]
35. Jeong, N.-R.; Han, S.-W.; Ko, B. Effects of Green Network Management of Urban Street Trees on Airborne Particulate Matter ($PM_{2.5}$) Concentration. *Int. J. Environ. Res. Public Health* **2023**, *20*, 2507. [CrossRef]
36. Penkała, M.; Rogula-Kozłowska, W.; Ogrodnik, P.; Bihałowicz, J.S.; Iwanicka, N. Exploring the Relationship between Particulate Matter Emission and the Construction Material of Road Surface: Case Study of Highways and Motorways in Poland. *Materials* **2023**, *16*, 1200. [CrossRef]
37. Ma, Y.; Zhao, H.; Liu, Q. Characteristics of $PM_{2.5}$ and PM_{10} pollution in the urbanagglomeration of Central Liaoning. *Urban Clim.* **2022**, *43*, 101170. [CrossRef]
38. Groma, V.; Alfoldy, B.; Borcsok, E.; Czompoly, O.; Füri, P.; Keri, A.H.; Kovacs, G.; Torok, S.; Osan, J. Sources and health effects of fine and ultrafine aerosol particles in an urban environment. *Atmos. Pollut. Res.* **2022**, *13*, 101302. [CrossRef]
39. Dai, H.; Huang, G.; Zeng, H.; Yu, R. Haze Risk Assessment Based on Improved PCA-MEE and ISPO-LightGBM Model. *Systems* **2022**, *10*, 263. [CrossRef]
40. Dai, H.; Huang, G.; Wang, J.; Zeng, H. VAR-tree model based spatio-temporal characterization and prediction of O_3 concentration in China. *Ecotoxicol. Environ. Saf.* **2023**, *257*, 114960. [CrossRef]
41. Coelho, M.S.; Zacharias, D.C.; de Paulo, T.S.; Ynoue, R.Y.; Fornaro, A. Air Quality Impact Estimation Due to Uncontrolled Emissions from Capuava Petrochemical Complex in the Metropolitan Area of São Paulo (MASP), Brazil. *Atmosphere* **2023**, *14*, 577. [CrossRef]
42. Molden, N.; Hemming, C.; Leach, F.; Levine, J.G.; Ropkins, K.; Bloss, W. Exposures to Particles and Volatile Organic Compounds across Multiple Transportation Modes. *Sustainability* **2023**, *15*, 4005. [CrossRef]
43. Arole, K.; Velhal, M.; Tajedini, M.; Xavier, P.G.; Bardasz, E.; Green, M.J.; Liang, H. Impacts of particles released from vehicles on environment and health. *TribolInt* **2023**, *184*, 108417. [CrossRef]
44. Cho, M.C.; Jo, Y.G.; Son, J.A.; Kim, I.; Oh, K.; Yook, S.J. Deposition characteristics of soot and tire-wear particles on urbantree leaves. *J. Aerosol. Sci.* **2021**, *155*, 105768. [CrossRef]
45. Jiaqiang, E.; Xu, W.; Ma, Y.; Tan, D.; Peng, Q.; Tan, Y.; Chen, L. Soot formation mechanism of modern automobile engines and methods of reducing soot emissions: A review. *Fuel Process Technol* **2022**, *235*, 107373. [CrossRef]
46. Arora, P.; Verma, P.; Lodi, F.; Jafari, M.; Zare, A.; Stevanovic, S.; Bodisco, T.A.; Brown, R.J.; Ristovski, Z. Particulate emissions and soot characterisation of diesel engine exhaust forsteady-state operating condition using dioctyl phthalate blends with diesel. *Fuel* **2023**, *340*, 127527. [CrossRef]
47. Sharma, A.; Mukut, K.M.; Roy, S.P.; Goudeli, E. The coalescence of incipient soot clusters. *Carbon* **2021**, *180*, 215–225. [CrossRef]
48. La Rocca, A.; Di Liberto, G.; Shayler, P.J.; Fay, M.W. The nanostructure of soot-in-oil particles and agglomerates from an automotive diesel engine. *Tribol. Int.* **2013**, *61*, 80–87. [CrossRef]
49. Bora, J.; Deka, P.; Bhuyan, P.; Sarma, K.P.; Hoque, R.R. Morphology and mineralogy of ambient particulate matter over mid-Brahmaputra Valley: Application of SEM–EDX, XRD, and FTIR techniques. *SN Appl. Sci.* **2021**, *3*, 137. [CrossRef]
50. Usman, F.; Zeb, B.; Alam, K.; Huang, Z.; Shah, A.; Ahmad, I.; Ullah, S. In-Depth Analysis of Physicochemical Properties of Particulate Matter (PM_{10}, $PM_{2.5}$ and PM_1) and Its Characterization through FTIR, XRD and SEM–EDX Techniques in the Foothills of the Hindu Kush Region of Northern Pakistan. *Atmosphere* **2022**, *13*, 124. [CrossRef]
51. Kiefer, J.; Stärk, A.; Kiefer, A.L.; Glade, H. Infrared Spectroscopic Analysis of the Inorganic Deposits from Water in Domestic and Technical Heat Exchangers. *Energies* **2018**, *11*, 798. [CrossRef]
52. Varrica, D.; Tamburo, E.; Vultaggio, M.; Di Carlo, I. ATR–FTIR Spectral Analysis and Soluble Components of PM_{10} And $PM_{2.5}$ Particulate Matter over the Urban Area of Palermo (Italy) during Normal Days and Saharan Events. *Int. J. Environ. Res. Public Health* **2019**, *16*, 2507. [CrossRef]
53. Zeb, B.; Alam, K.; Sorooshian, A.; Blaschke, T.; Ahmad, I.; Shahid, I. On the morphology and composition of particulate matter in an urban environment. *Aerosol Air Qual. Res.* **2018**, *18*, 1431–1447. [CrossRef]
54. Koupadi, K.; Boyatzis, S.C.; Roumpou, M.; Kalogeropoulos, N.; Kotzamani, D. Organic Remains in Early Christian Egyptian Metal Vessels: Investigation with Fourier Transform Infrared Spectroscopy and Gas Chromatography–Mass Spectrometry. *Heritage* **2021**, *4*, 3611–3629. [CrossRef]
55. Kim, E.A.; Koh, B. Utilization of road dust chemical profiles for source identification and human health impact assessment. *Sci. Rep.* **2020**, *10*, 14259. [CrossRef]
56. Formenton, G.; Bassetto, A.; De Lorenzo, R. Determination of Volatile Organic Compounds in Air byGC/MS: Italian Proficiency Tests. *J. AOAC Int.* **2013**, *96*, 178–185. [CrossRef] [PubMed]

57. Orecchio, S.; Fiore, M.; Barreca, S.; Vara, G. Volatile Profiles of Emissions from DifferentActivities Analyzed Using Canister Samplersand Gas Chromatography-Mass Spectrometry(GC/MS) Analysis: A Case Study. *Int. J. Environ. Res. Public Health* **2017**, *14*, 195. [CrossRef] [PubMed]
58. Navazo, M.; Durana, N.; Alonso, L.; García, J.A.; Ilardia, J.L.; Gómez, M.C.; Gangoiti, G. Volatile organic compounds in urban and industrial atmospheres: Measurement techniques and data analysis. *Int. J. Environ. Anal. Chem.* **2003**, *83*, 199–217. [CrossRef]
59. Jin, H.; Yuan, W.; Li, W.; Yang, J.; Zhou, Z.; Zhao, L.; Li, Y.; Qi, F. Combustion chemistry of aromatic hydrocarbons. *Prog. Energy Combust. Sci.* **2023**, *96*, 101076. [CrossRef]
60. Saarikoski, S.; Hellén, H.; Praplan, A.P.; Schallhart, S.; Clusius, P.; Niemi, J.V.; Kousa, A.; Tykkä, T.; Kouznetsov, R.; Aurela, M.; et al. Characterization of volatile organic compounds and submicron organic aerosol in a traffic environment. *Atmos. Chem. Phys.* **2023**, *23*, 2963–2982. [CrossRef]